Since January 2020 Elsevier has created a COVID-19 resource centre with free information in English and Mandarin on the novel coronavirus COVID-19. The COVID-19 resource centre is hosted on Elsevier Connect, the company's public news and information website.

Nano Today 40 (2021) 101280

Contents lists available at ScienceDirect

Nano Today

journal homepage: www.elsevier.com/locate/nanotoday

Systemic antiviral immunization by virus-mimicking nanoparticles-decorated erythrocytes

Lu Wang[a], Xinyue Wang[a], Fengmin Yang[a], Ying Liu[a], Lu Meng[b], Yan Pang[c,*], Mengmeng Zhang[a], Fangjie Chen[a], Chao Pan[a], Sisi Lin[a], Xinyuan Zhu[b,*], Kam W. Leong[d], Jinyao Liu[a,*]

[a] Shanghai Key Laboratory for Nucleic Acid Chemistry and Nanomedicine, Institute of Molecular Medicine, State Key Laboratory of Oncogenes and Related Genes, Shanghai Cancer Institute, Renji Hospital, School of Medicine, Shanghai Jiao Tong University, Shanghai 200127, China
[b] School of Chemistry and Chemical Engineering, State Key Laboratory of Metal Matrix Composites, Shanghai Jiao Tong University, Shanghai 200240, China
[c] Department of Ophthalmology, Shanghai Ninth People's Hospital, School of Medicine, Shanghai Jiao Tong University, Shanghai 200011, China
[d] Department of Biomedical Engineering, Columbia University, New York, NY, USA

ARTICLE INFO

Article history:
Received 2 May 2021
Received in revised form 22 July 2021
Accepted 23 August 2021
Available online 4 September 2021

Keywords:
virus-mimicking nanoparticles
erythrocytes
vaccine
antiviral immunity
COVID-19

ABSTRACT

New vaccine technologies are urgently needed to produce safe and effective vaccines in a more timely manner to prevent future infectious disease pandemics. Here, we describe erythrocyte-mediated systemic antiviral immunization, a versatile vaccination strategy that boosts antiviral immune responses by using erythrocytes decorated with virus-mimetic nanoparticles carrying a viral antigen and a Toll-like receptor (TLR) agonist. As a proof of concept, polydopamine nanoparticles were synthesized via a simple in situ polymerization in which the nanoparticles were conjugated with the SARS-CoV-2 spike protein S1 subunit and the TLR7/8 agonist R848. The resulting SARS-CoV-2 virus-mimetic nanoparticles were attached to erythrocytes via catechol groups on the nanoparticle. Erythrocytes naturally home to the spleen and interact with the immune system. Injection of the nanoparticle-decorated erythrocytes into mice resulted in greater maturation and activation of antigen-presenting cells, humoral and cellular immune responses in the spleen, production of S1-specific immunoglobulin G (IgG) antibodies, and systemic antiviral T cell responses than a control group treated with the nanoparticles alone, with no significant negative side effects. These results show that erythrocyte-mediated systemic antiviral immunization using viral antigen- and TLR agonist-presenting polydopamine nanoparticles-a generalizable method applicable to many viral infections-is effective new approach to developing vaccines against severe infectious diseases.

Introduction

Vaccination prevents infection by stimulating the immune system to attack specific antigens [1], and mass vaccination prevents the spread of infectious disease. Improvements in vaccine technology have yielded vaccines that boost effective immunity against newly emerging infectious diseases [2,3], but the spread of new infectious diseases still outpaces vaccine development. COVID-19 has caused more than 140 million confirmed infections with a 2.1% mortality rate as of April 2021 [4]. The high infection rate of SARS-CoV-2 (40-fold higher than that of SARS-CoV-1) [5], the high mortality rate of COVID-19, and the high frequency of asymptomatic infections have created an urgent demand for vaccines that has not been satisfied even by the improved speed of new vaccine development [6]. To prevent or mitigate future infectious disease pandemics, new vaccine technologies are needed that allow rapid production of safe and effective vaccines.

Conventional vaccines employ attenuated or inactivated viruses, viral vectors, recombinant protein antigens, or nucleic acids that encode viral antigens [7]. Each of these approaches has limitations [8]. For attenuated viruses, extensive additional testing is required to verify their safety due to the risk of reversion to virulence [9]. For inactivated viruses, their lowered immunogenicity requires the use of adjuvants, and widely used adjuvants such as alum produce only a humoral immune response [10]. For adenoviruses (the most common viral vector), pre-existing immunity can dampen the immunogenicity of the vaccine [11]. For vaccines that employ proteins and nucleic acids, instability during preparation, storage, transport,

* Corresponding authors.
E-mail addresses: yanpang@shsmu.edu.cn (Y. Pang), xyzhu@sjtu.edu.cn (X. Zhu), jyliu@sjtu.edu.cn (J. Liu).

https://doi.org/10.1016/j.nantod.2021.101280
1748-0132/

and administration restricts broad implementation [7], and in vivo degradation and biological barriers limit accumulation of the therapeutic proteins and nucleic acids at the desired sites [12,13].

Vaccines that employ virus-mimetic nanoparticles (VNPs) to present viral antigens have shown promising safety and effectiveness [7]. Nanoparticles can be engineered to target specific tissues and cell types to improve targeted accumulation, and to deliver viral antigens together with molecular adjuvants that boost protective humoral and cellular immune responses [14]. Nanoparticle carriers can also improve the stability of their cargo [15]. These characteristics make nanoparticles well-suited for use in vaccines against pathogens that have been characterized genetically and structurally [16,17]. However, nanoparticle vaccines penetrate biological barriers and tissues passively by diffusion [14], and most nanoparticles are rapidly eliminated by the mononuclear phagocyte system before entering into the draining lymph nodes or being captured by tissue-resident antigen-presenting cells (APCs), reducing the efficiency of antigen presentation to lymphocytes [18]. Therefore, methods that specifically and effectively deliver VNPs to secondary lymphoid organs such as the spleen are needed.

The spleen is a secondary lymphoid organ along with the lymph nodes. Its primary functions are to filter pathogens from circulation [19] to generate immune responses to blood-borne antigens [20], and to remove abnormal erythrocytes. Erythrocytes home to the spleen and are phagocytosed once they reach the end of their lifespan [21]. Erythrocytes capture and deactivate microorganisms in blood, then present the captured pathogens to professional APCs in the spleen [22,23]. Despite the mechanism of cargo uptake by APCs has not been well-understood yet, the alteration of complement receptor 1 (CR1) on erythrocytes has been reported to have a stimulatory effect on particle binding and uptake [24]. These natural functions of erythrocytes have been leveraged elegantly to carry therapeutic payloads such as nanoparticle-based therapeutics for targeted transport [25–27], including delivery of antigens to splenic APCs [28]. Therefore erythrocytes are promising candidates for delivery of VNPs in a vaccine.

Here, we report a strategy called erythrocyte-mediated antiviral immunization in which erythrocytes are decorated with polydopamine nanoparticles that present a viral antigen and a Toll-like receptor (TLR) agonist to produce systemic antiviral immunity with both humoral and cellular immune responses (Fig. 1). The viral antigen and TLR agonist are attached to the nanoparticles during in situ oxide-induced self-polymerization of dopamine. Catechol groups on the nanoparticle surface enable immobilization onto the erythrocyte membrane. As a proof of concept, we decorated erythrocytes with nanoparticles presenting the SARS-CoV-2 spike protein S1 subunit and the TLR7/8 agonist R848, and evaluate the effectiveness of this vaccination approach in terms of maturation and activation of professional APCs, humoral and cellular immune responses in the spleen, systemic side effects, production of anti-S1 antibodies, and type 1 interferon-mediated antiviral T cell response.

Results and discussion

Design and preparation of virus-mimetic nanoparticles

We chose the SARS-CoV-2 spike protein S1 subunit [29–31] as a model viral antigen for this proof-of-concept study since previous SARS/MERS vaccines have demonstrated the effectiveness of S1 as a viral antigen. Other effective antigens include full-length S protein and the S protein subunits RBD and S2 [32]. We selected R848, an imidazoquinoline and agonist of TLRs 7 and 8 that mimics pathogen-associated molecular patterns such as single-stranded RNA which induce innate immunity against viral infections [33]. TLR agonists in vaccines improve antibody production and enhance immune responses [34,35]. We hypothesized that nanoparticles presenting S1 and R848 would elicit a similar immune response as infection with SARS-CoV-2, which is an enveloped, positive-sense, and single-stranded RNA virus [36].

Polydopamine nanoparticles (PDA-NPs) can be easily obtained by stirring dopamine monomer in an aerobic alkaline solution [37]. The abundant active catechol groups in the nanoparticles allow conjugation of diverse molecules containing nucleophilic groups such as primary amines and thiols via Michael addition and Schiff base reactions [38]. S1 protein and R848 were mixed with dopamine monomer in an alkaline buffer to synthesize the S1/R848-presenting VNPs (Fig. 2a), followed by purification by centrifugation. This synthesis is simple and no organic solvent is used.

Transmission electron microscopy (TEM) images of both PDA-NPs and VNPs showed spherical structures with a narrow size distribution. VNPs appeared slightly larger and with a rougher surface than PDA-NPs via TEM (Fig. 2b, c). The average size of the particles was 170 ± 44 nm for the PDA-NPs, and 195 ± 81 nm for the VNPs, based on dynamic light scattering (DLS) analysis (Figs. 2d and S1). With the introduction of the negatively charged S1 protein, the zeta potential of the nanoparticles decreased dramatically, from −1.96 ± 4.84 for the PDA-NPs to −34.20 ± 5.87 mV for the VNPs (Fig. 2e). As shown in Fig. S2, the particle size of VNPs remained stable during this period, which implied a satisfactory storage stability. To confirm grafting of S1 onto the nanoparticles, S1 was labeled with Rhodamine B (RhB) and the nanoparticles were observed with confocal laser scanning microscopy (CLSM). Distinct fluorescence signals were associated with VNPs but not PDA-NPs, indicating incorporation of S1 in the VNPs (Fig. S3). Flow cytometric analysis confirmed conjugation of S1 (Fig. 2f, g). S1 antigen loading was 15 wt% based on the change in protein concentration in the reaction solution following polymerization (Fig. S4a). Incorporation of R848 was confirmed by the presence of a characteristic absorption peak at 320 nm in the ultraviolet-visible (UV–vis) spectra of the VNPs (Fig. S4b) and a standard calibration curve of R848 (Fig. S4c). The loading of R848 increased from 2 to 25 wt% as the R848 concentration in the reaction solution increased from 50 to 200 μg/mL (Fig. 2h, i).

Anchoring virus-mimetic nanoparticles onto erythrocytes

We implemented erythrocyte-mediated systemic antiviral immunization against SARS-CoV-2 infection by anchoring erythrocytes with VNPs that present the antigenic SARS-CoV-2 S1 protein and the TLR7/8 agonist R848 to mimic the immune response induced by infection with SARS-CoV-2. The attachment of S1/R848-functionalized nanoparticles onto the surface of the erythrocytes was accomplished in a simple single-step reaction by mixing the VNPs and erythrocytes (Fig. 3a). To characterize the conjunction of VNPs with erythrocytes, the nanoparticles were labeled with fluorescein isothiocyanate (FITC) and the VNP-decorated cells were imaged by CLSM. CLSM images showed numerous green fluorescent dots concentrated on VNP-erythrocytes which were not be observed on bare erythrocytes (Figs. 3b and S5). Scanning electron microscope (SEM) images indicated that VNPs were anchored to the VNP-erythrocytes, and there was no significant change in cell morphology after

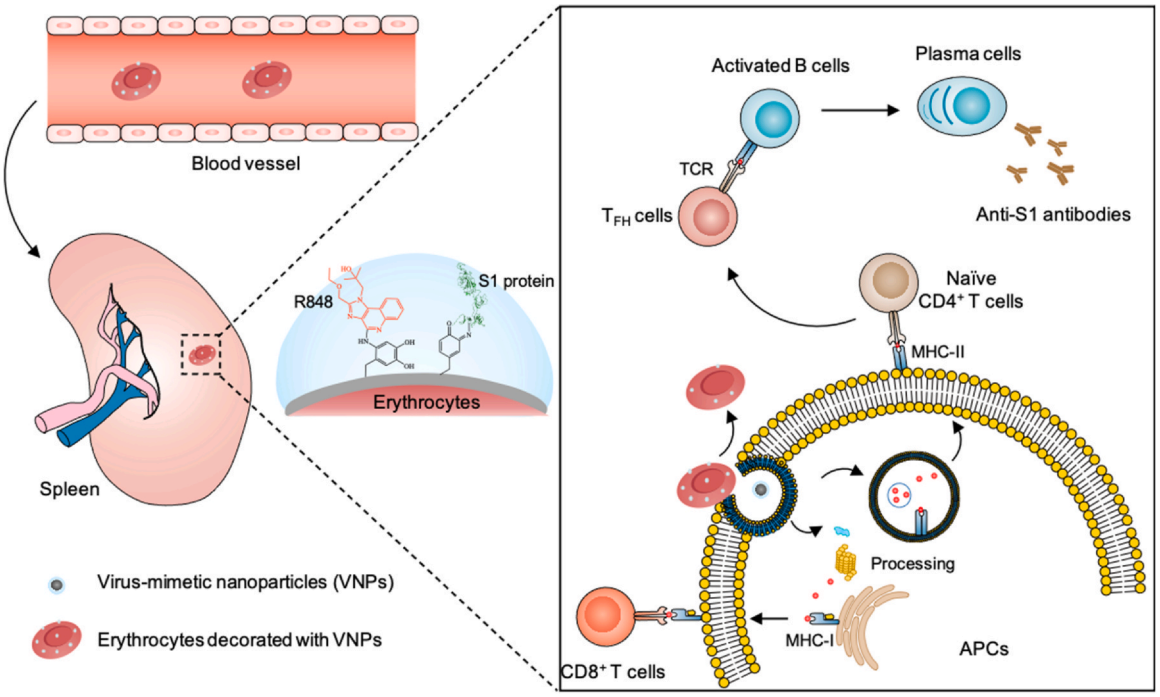

Fig. 1. Erythrocyte-mediated systemic antiviral immunization. A systemic antiviral immune response is elicited by erythrocytes decorated with virus-mimetic nanoparticles (VNPs) that present the antigenic SARS-CoV-2 spike protein S1 subunit and the TLR7/8 agonist R848. The innate functions of erythrocytes include spleen enrichment and immune system interactions. VNP-decorated erythrocytes induce the maturation of antigen-presenting cells and robust humoral and cellular immune responses in the spleen.

modification (Fig. 3c). TEM showed a uniform distribution of VNPs on the cell surface (Figs. 3d and S6). Image J was used to calculate the number of VNPs on the surface of erythrocytes. The results showed that the average VNP number on each erythrocyte was 120–150 (Fig. S7). Flow cytometry analysis confirmed conjugation of the cells with VNPs (Fig. 3e). Limited aggregation is a prerequisite for systemic administration [39]. No visible aggregation occurred when using erythrocyte-to-VNP ratios from 1:30 to 1:240 based on a visual agglutination assay. Agglutination was observed at 1:480 (Fig. 3f). We further quantified the modification of cell membranes with VNPs by testing the expression of phosphatidylserine and the level of CD47 on the cell membrane. The expression of phosphatidylserine increased dramatically at erythrocyte-to-VNP ratios of 1:210, 1:240, and 1:480 (Figs. 3g and S8). As shown in Fig. S9, the CD47 expression of VNP-erythrocytes was observed lower than that of erythrocytes, which could be ascribed to the shielding effect of VNPs. Modification of erythrocyte membranes with VNPs could promote their accumulation in the spleen by leveraging the spleen's function of removing abnormal erythrocytes [28].

Maturation and activation of APCs by VNP-decorated erythrocytes

Dendritic cells (DCs) are the most potent APCs [40]. In vaccination, antigen uptake by immature DCs initiates adaptive immune responses, and combination with adjuvants can amplify the immunization [10,41]. After antigen capture, DCs mature and become fully functional APCs with upregulation of costimulatory molecules, the major histocompatibility complex (MHC), and cytokine secretion [42]. To assess the capacity of VNP-erythrocytes to activate APCs, we co-cultured VNP-erythrocytes with induced bone marrow-derived dendritic cells (BMDCs). PBS, PDA-NPs, and unmodified erythrocytes were used as negative controls. VNP and R848 alone were positive controls. After an overnight co-incubation, the cells were analyzed by flow cytometry. Cells treated with R848 exhibited a more than two-fold higher percentage of mature BMDCs ($CD80^+CD86^+$) than the negative controls (Figs. 4a and S10, S11). Co-culture with VNPs and VNP-erythrocytes further increased BMDC maturation, which was consistent with previous studies showing that co-delivery of antigens and adjuvants promoted APC maturation [43]. Expression levels of the costimulatory molecules CD80 and CD86 on BMDCs incubated with R848 were significantly higher than on BMDCs in the PBS, PDA-NP, and unmodified erythrocyte groups (Fig. 4b, c). Co-culture of BMDCs with VNPs and VNP-erythrocytes increased the expression levels of CD80 and CD86. Co-culture with VNP-erythrocytes caused a greater increase in CD80 expression than treatment with VNPs alone (Fig. 4b). Increases in CD80 expression have been shown to be important for maintaining T cell responses [44,45]. The maturation and activation of BMDCs by co-incubation with VNP-erythrocytes is also consistent with previous studies using erythrocytes conjugated with nanoparticles [28].

Antigen presentation might be augmented by uptake of VNPs that have detached from erythrocytes. To investigate this hypothesis, flow cytometric analysis and CLSM imaging were performed to measure cellular uptake of VNPs containing fluorescently-labeled S1. The results indicated a dramatic increase with incubation time in fluorescence intensity (Figs. 4d, e and S12). CLSM images confirmed that RhB-labeled S1 was endocytosed into the cytoplasm of DCs after 6 h of co-culture (Fig. 4f and S13).

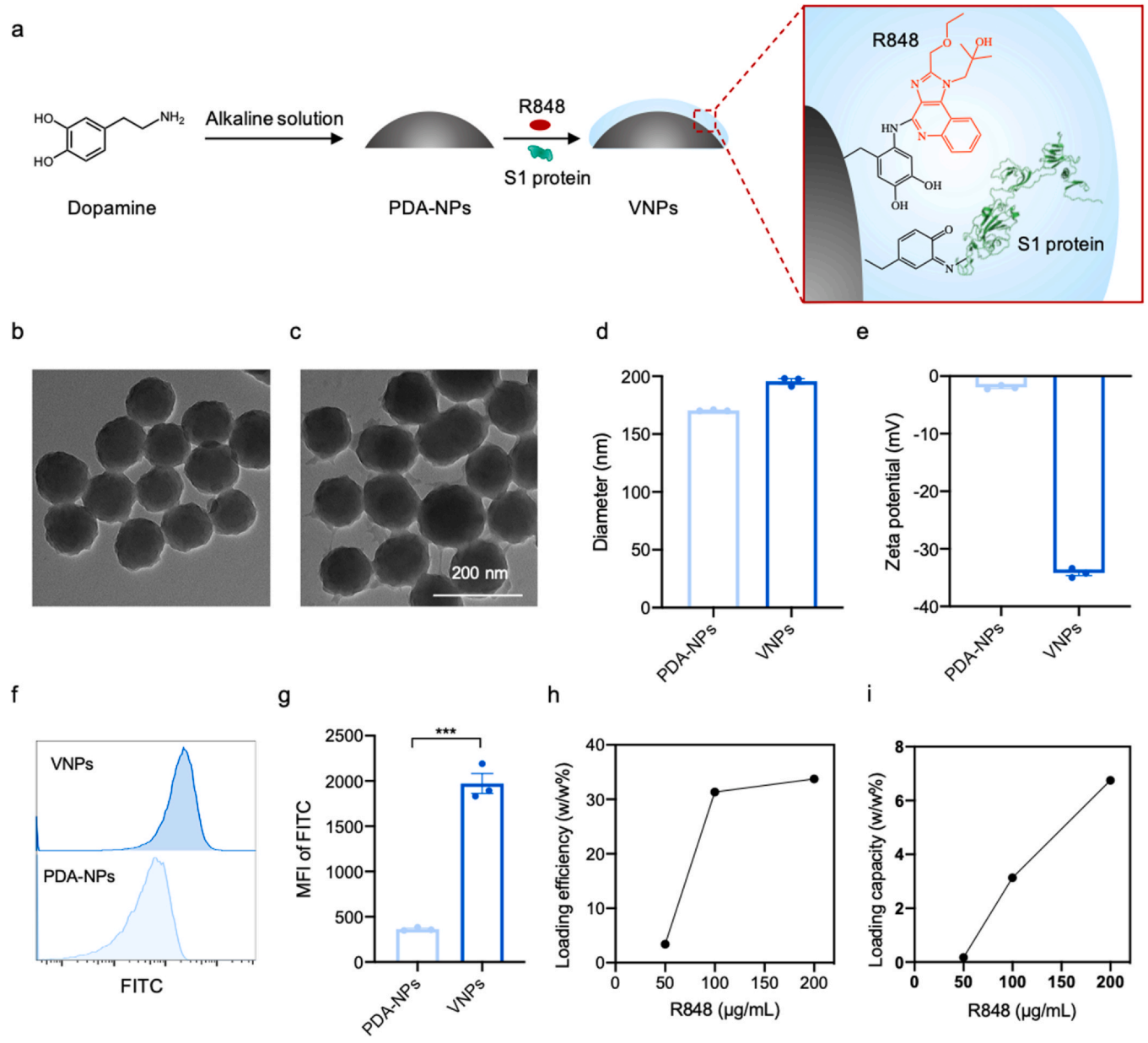

Fig. 2. Preparation and characterization of virus-mimetic nanoparticles. (a) Schematic of the preparation of VNPs by conjugating antigenic proteins and agonists with polydopamine nanoparticles via in situ polymerization. Gray and blue means PDA-NPs and the attached adjuvant and antigen, respectively. (b, c) TEM images of PDA-NPs (b) and VNPs (c). Scale bar, 200 nm. (d, e) Size distribution (d) and zeta potential (e) of PDA-NPs and VNPs measured by DLS. (f, g) Flow cytometry histograms (f) and mean fluorescence intensity (MFI) (g) of PDA-NPs without S1 and VNPs with FITC-labeled S1. Data are mean ± SEM ($n = 3$). Statistical analysis was performed using Student's *t*-test; $^{***}P < 0.001$. (h, i) Loading efficiency (h) and loading capacity (i) of R848 in VNPs at different feed concentrations measured by UV/vis spectrophotometry. Data are mean ± SEM ($n = 3$).

Blood circulation and accumulation in the spleen

We next evaluated the pharmacokinetics of RhB-labeled VNP-erythrocytes by collecting and analyzing peripheral blood sampled from mice at 2, 4, 8, 20, 30, and 48 h after intravenous injection. Blood samples were examined by flow cytometry to measure the percentage and fluorescence intensity of erythrocytes presenting RhB signal. Limited variation in the percentage of RhB^+ erythrocytes in peripheral blood was observed between these time points (Fig. 4g). Interestingly, the fluorescence intensity of VNP-erythrocytes decreased steadily over this period (Fig. 4h). To confirm the release of VNPs by VNP-erythrocytes, we measured the amount of fluorescence due to RhB-labeled VNPs on the surface of the erythrocytes. The fluorescence intensity of VNP-erythrocytes decreased when incubated in PBS with 20% mouse serum at 37 ℃ (Fig. 4i, j). The disassociation of VNPs from erythrocytes was also directly visualized

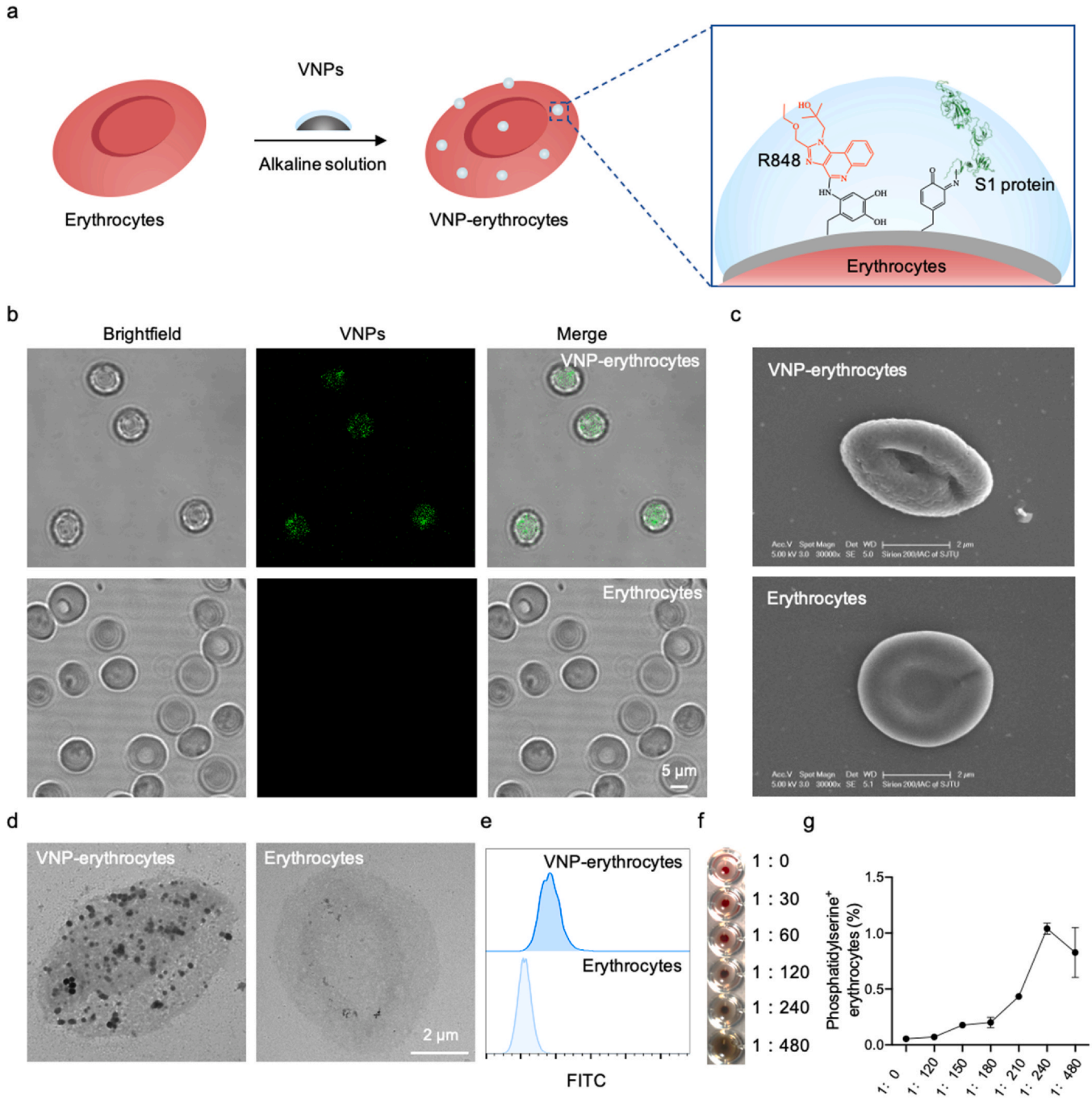

Fig. 3. Preparation and characterization of VNP-decorated erythrocytes. (a) Schematic of binding VNPs with erythrocytes. Gray and blue separately indicate PDA-NPs and the attached adjuvant and antigen. (b) CLSM images of VNP-erythrocytes (top) and unmodified erythrocytes (bottom). VNPs were labeled with FITC (green). Scale bar, 5 μm. (c, d) SEM (c) and TEM (d) images of VNP-erythrocytes and erythrocytes. Scale bar, 2 μm. (e) Flow cytometry histograms of unmodified erythrocytes and VNP-erythrocytes with FITC-labeled VNPs. (f, g) Visual agglutination assay (f) and phosphatidylserine expression (g) of erythrocytes after binding with different ratios of VNPs. Data are mean ± SEM ($n = 4$).

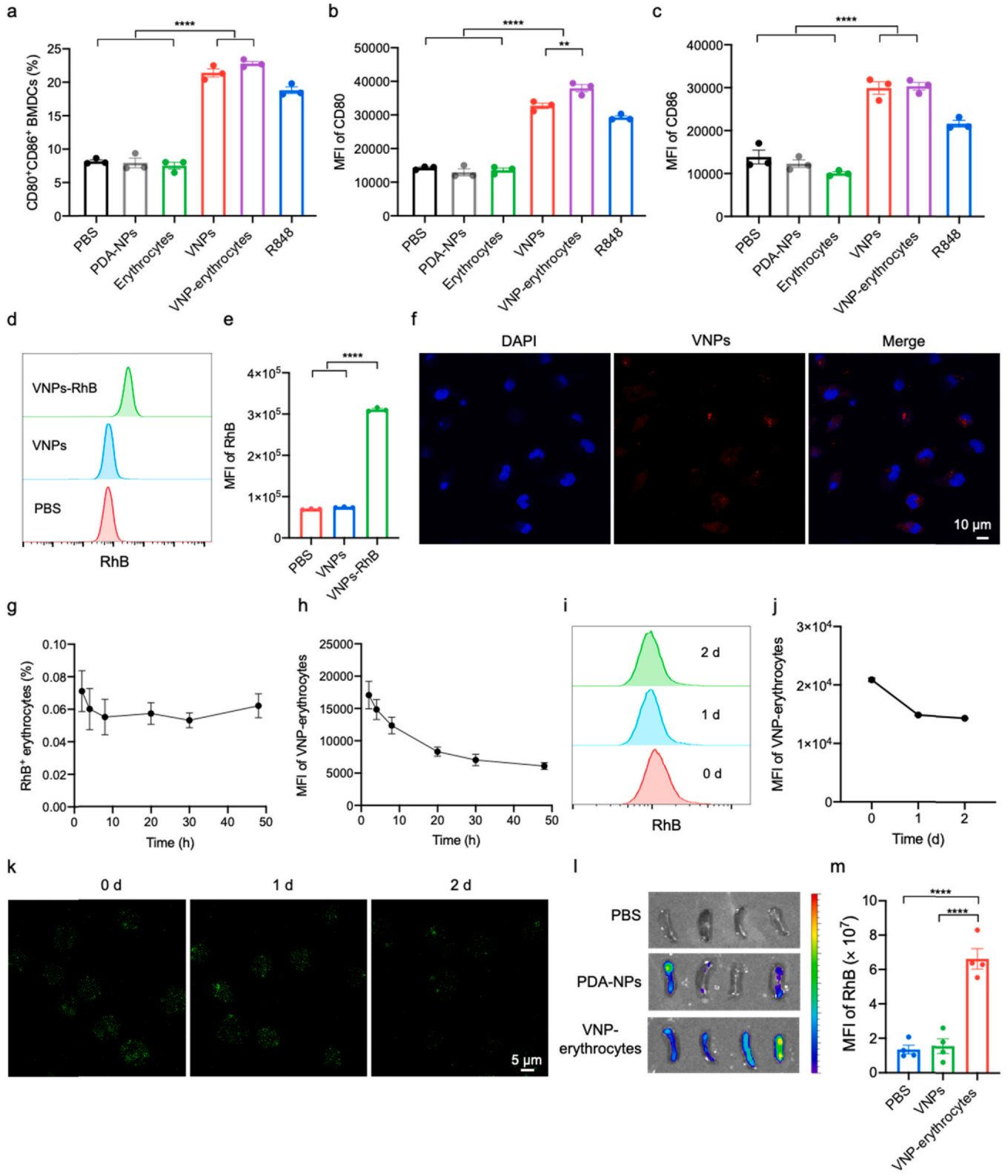

Fig. 4. Immunogenicity, blood circulation, and spleen enrichment of VNP-erythrocytes. (a-c) Percentage of mature BMDCs ($CD80^+CD86^+$) (a), MFI quantification of costimulatory markers CD80 (b) and CD86 (c) analyzed by flow cytometry after different stimulations for 24 h. Statistical analysis was performed using one-way ANOVA with the Tukey's post-test ($n = 3$); $^{**}P < 0.01$, $^{****}P < 0.0001$. (d-f) Flow cytometry histograms (d), MFI (e), and CLSM images (f) of DC2.4 cells after incubation with RhB-labeled VNPs for 6 h. Statistical analysis was performed using one-way ANOVA with the Tukey's post-test ($n = 3$); $^{****}P < 0.0001$. Scale bar, 5 μm. (g, h) Kinetics of percentage of VNP-erythrocytes in peripheral blood total erythrocytes (g) and MFI of VNP-erythrocytes in peripheral blood (h) over 48 h after intravenous injection in mice. Data are mean ± SEM ($n = 5$). (i-k) Shedding kinetics of VNPs from VNP-erythrocytes determined by flow cytometric analysis (i), MFI quantification (j) and CLSM imaging (k) at 37 °C in PBS contained 10% mouse serum. Scale bar, 5 μm. (l, m) IVIS images (l) and MFI (m) of the spleens harvested from mice 2 days after injection. Scale indicates low (blue) to high (red) radiant efficiency. Statistical analysis was performed using one-way ANOVA with the Tukey's post-test ($n = 4$); $^{****}P < 0.0001$.

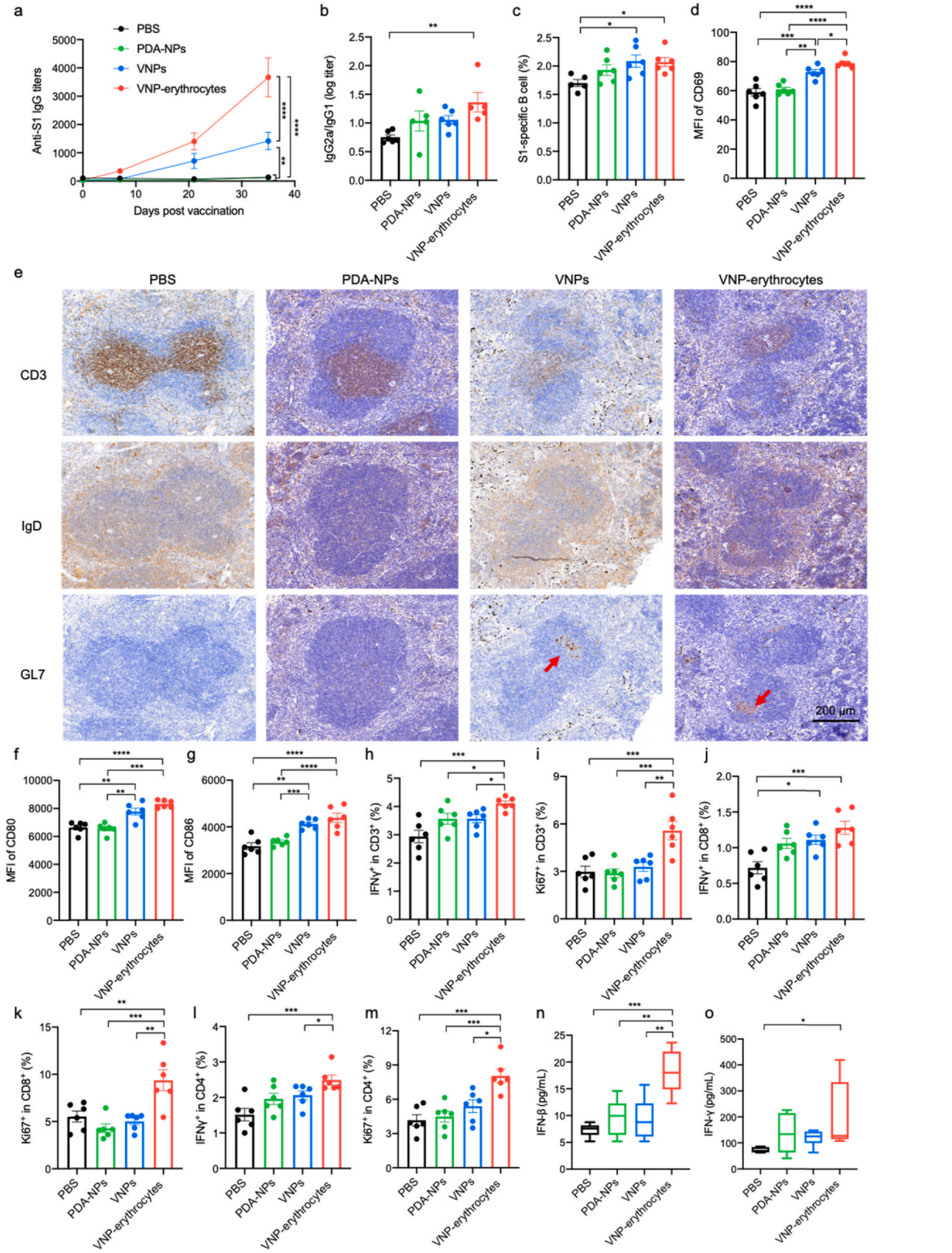

caption on nest page

Fig. 5. Immune responses elicited by erythrocyte-mediated antiviral immunization. (a, b) Kinetics of SARS-CoV-2 S1-specific IgG antibody titers (a) and ratio of IgG2a/IgG1 at day 21 (b) in serum assessed by ELISA after immunization mice with PBS, PDA-NPs, VNPs, and VNP-erythrocytes via intravenous injection on days 0, 7, and 14 ($n = 6$). (c) Percentage of SARS-CoV-2 S1-specific B cells analyzed by flow cytometry. Cells were stained with SARS-CoV-2 S1-his protein and anti-his antibody labeled with PE. (d) MFI quantifications of activation marker CD69 on B cells. (e) Immunohistochemical staining of CD3, IgD, and GL7 in the spleen. Red arrows indicate GC B cells. Scale bar, 200 μm. (f, g) MFI quantification of costimulatory markers CD80 (f) and CD86 (g) on DCs. (h-m) Total T cell (h, i), $CD8^+$ T cell (j, k) and $CD4^+$ T cell (l, m) responses in the spleen determined by intracellular IFN-γ and Ki67 staining. (n, o) IFN-β (n) and IFN-γ (o) levels in serum of immunized mice measured by ELISA. Statistical analysis was performed using two-way ANOVA with the Bonferroni correction post-test and one-way ANOVA with the Tukey's post-test ($n = 6$); $^*P < 0.05$, $^{**}P < 0.01$, $^{***}P < 0.001$, $^{****}P < 0.0001$.

by CLSM. The number of green fluorescent dots indicating FITC-labeled VNPs on erythrocytes decreased with incubation time up to 48 h (Fig. 4k).

To assess the ability of VNP-erythrocytes to accumulate in the spleen, mice were intravenously injected with 100 μL of RhB-VNP-erythrocytes. PBS and RhB-labeled VNPs without erythrocytes were used as controls. Two days after injection, the detection of fluorescence intensity of RhB in peripheral blood displayed a prolonged blood circulation for anchored VNPs compared to free VNPs (Fig. S14). Meanwhile, spleens were harvested from mice and imaged with an in vivo imaging system (IVIS). In contrast to free VNPs, fluorescence images and quantitative analysis showed a significantly enhanced accumulation of VNP-erythrocytes in the spleen (Fig. 4l, m). These results indicated that the erythrocytes afforded an effective depot [46] for the vaccine components with a long circulation time, which could improve the distribution of the vaccine in the spleen and stimulate an enhanced immune response.

Eliciting of humoral and cellular immune responses

Having confirmed spleen enrichment as well as BMDC maturation and activation, we evaluated the immunogenicity of VNP-erythrocytes in a mouse model. C57BL/6 mice were injected intravenously with PBS, PDA-NPs, VNPs, or VNP-erythrocytes (Fig. S15). After prime-boost vaccinations on days 0, 7, and 14, serum was collected on days 7, 21, and 35 for ELISA analysis. VNP-erythrocytes evoked significantly higher titers of anti-S1 immunoglobulin G (IgG) than all other groups (Figs. 5a and S16). The ratio of IgG2a to IgG1 antibody titers is an indicator of Th1 and Th2 bias [47]. The IgG2a/IgG1 ratio of VNP-erythrocyte-immunized mice was significantly higher than that of other groups (Fig. 5b), suggesting that the VNP-erythrocytes initiated a Th1-polarized protective immune response [48]. The spleens of immunized mice were harvested and homogenized on day 35 to analyze the activation and production of antigen-specific B cells, which is critical for induction of antibody-mediated immune responses [49]. VNPs alone and VNP-erythrocytes increased the percentage of S1-specific B cells (Fig. 5c). Notably, the VNP-erythrocyte group showed significantly higher expression of CD69 on B cells than the VNP-only group (Fig. 5d). The induction of CD69, an early activation marker of B cells, indicated the promoted B-cell proliferation and immunoglobulin production [50]. Germinal center (GC) formation in the spleen and lymph nodes is important for long-lived T cell-dependent humoral immunity [51]. The formation of GCs in the spleen of immunized mice was confirmed by immunohistochemical staining. Mice immunized with VNP-erythrocytes formed $GL7^+$ GC B cells in their spleens, unlike mice in the PBS and PDA-NP groups (Fig. 5e). These results demonstrated that the erythrocyte-mediated antiviral immunization evoked a humoral immune response.

The mean fluorescence intensities of CD80 and CD86 expressed by DCs were higher in mice treated with VNP-erythrocytes than in mice treated with the controls (Fig. 5f, g), indicating the importance of DC antigen presentation. T cell-mediated immunity plays a critical role in preventing SARS-CoV-2 infection [52]. $CD8^+$ T cells can be attracted into an infected site to kill invading cells, while $CD4^+$ T cells help prime B cells and produce cytokines [53]. Therefore, we evaluated the T cell properties after vaccination. The levels of interferon-gamma (IFN-γ) production and Ki67 expression in $CD3^+$ T cells in the spleen were significantly higher in the VNP-erythrocyte group than in the other groups, indicating that the VNP-erythrocytes promoted T cell activation and proliferation (Figs. 5h, i and S17a, b). The VNP-erythrocytes promoted the activation and proliferation of both $CD8^+$ and $CD4^+$ T cells (Figs. 5l-m and S17c-f), indicating that S1 epitopes were presented by the MHC-I and MHC-II of DCs. IFN-γ is a crucial immunomodulatory cytokine for resistance to multiple pathogens [54,55], and IFN-β is a type 1 IFN that is essential for controlling viral infections [56,57]. Treatment with VNP-erythrocytes achieved upgraded secretions of IFN-β, IFN-γ, and IL-6 in the serum (Figs. 5n, o and S18), demonstrating that the erythrocyte-mediated antiviral immunization initiated a strong systemic antiviral immune response. Collectively, the assistance of erythrocytes could prime T-cell and B-cell responses, leading to robust antibody production. These advantages could be attributed to the erythrocyte-mediated prolonged circulation in the blood, enhanced accumulation in the spleen, and improved antigen uptake by DCs.

Safety assessment

We assessed the safety of VNP-erythrocytes in vitro and in vivo. To evaluate cytotoxicity, HEK 293T cells were incubated with VNP-erythrocytes at a 5:1 ratio for 24 h and were stained with Annexin V and propidium iodide for imaging by CLSM. The amount of apoptosis induced by VNP-erythrocytes was similar to that induced by PBS, PDA-NPs, and VNPs (Fig. 6a), indicating negligible cytotoxicity. Flow cytometric analysis of the apoptosis rate showed a comparable percentage of annexin V^+ cells in the VNP-erythrocyte group as in the PBS group (Fig. 6b). This cytocompatibility may be due to the use of erythrocytes and the limited toxicity of polydopamine, which has been widely used in biomedical applications [58,59]. Cell viability was measured with a cell counting kit-8 (CCK8) assay. The viability of HEK 293T cells after exposure to different ratios of VNP-erythrocytes for 24 h was similar to the viability of cells incubated with PBS, PDA-NPs, or VNPs (Figs. 6c and S19), further indicating low cytotoxicity. We also monitored mouse body weight before and after vaccination and observed no fluctuation in body weight (Fig. 6d). Histological examination by hematoxylin and eosin (H&E) staining showed no detectable damage to major organs in all immunized mice (Fig. 6e), indicating the favorable safety of this vaccination method.

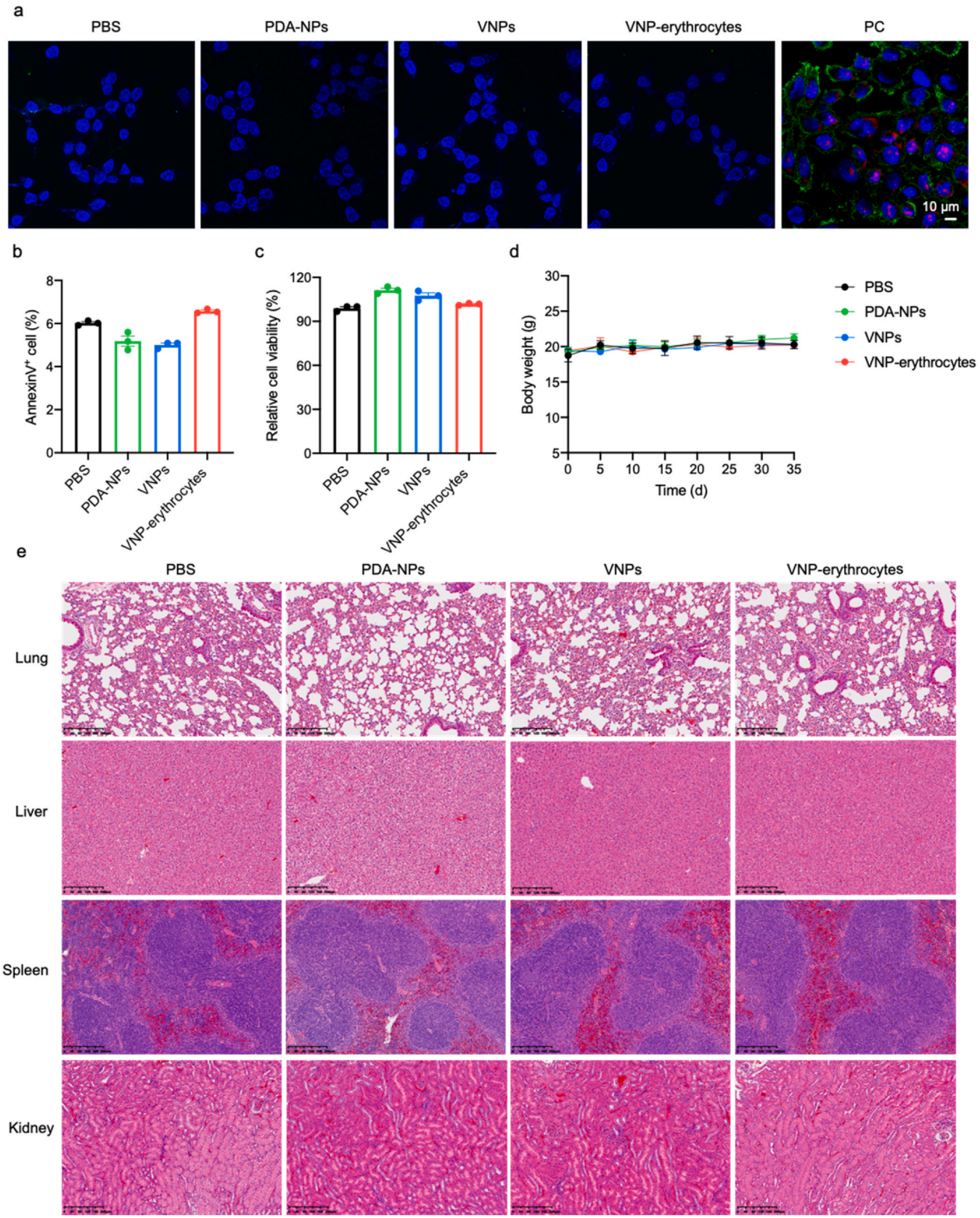

Fig. 6. Safety assessment. (a) CLSM images of apoptotic cells after incubation HEK 293T cells with PBS, PDA-NPs, VNPs, and VNP-erythrocytes for 24 h. PC indicates apoptosis positive control. Scale bar, 10 μm. (b, c) Percentages of cell apoptosis (b) and viability (c) of HEK 293T cells after exposure to different treatments for 24 h ($n = 3$). (d, e) Body weight (d) and H&E staining images (e) of the lung, liver, spleen, and kidney. Mice were separately immunized with PBS, PDA-NPs, VNPs, and VNP-erythrocytes on days 0, 7, and 14 and were sacrificed on day 21 for organ collection ($n = 6$). Scale bar, 200 μm.

Conclusion

In summary, we report the use of erythrocyte-mediated antiviral immunization with virus-mimetic polydopamine nanoparticles presenting viral antigen and a TLR agonist as a versatile and effective strategy to provoke robust antiviral immunity. This approach employs in situ polymerization of dopamine to incorporate viral antigens and TLR agonists in a nanoparticle. The synthesis method is simple and is suitable for loading other viral antigens due to the flexibility of polydopamine for conjugating structurally diverse molecules. Due to the innate ability of erythrocytes to accumulate in the spleen and interact with APCs, erythrocytes anchored with virus-mimicking nanoparticles deliver viral antigens effectively to splenic DCs and activate potent humoral and cellular immune responses upon systemic administration. Treatment with erythrocytes bearing SARS-CoV-2-mimetic nanoparticles presenting the S1 antigen and the TLR7/8 agonist R848 elicited adequate production of specific IgGs and a systemic antiviral T cell response with limited side effects. Despite substantial advances in the laboratory settings, batch-to-batch variation in preparation of VNP-erythrocytes, stability for long-term storage, pressure on the demand for erythrocytes, and patient reluctance to intravenous injection need to be considered for future translation. Moreover, further studies are needed to evaluate the biosafety of this erythrocyte-mediated antiviral immunization method in large animal models and to optimize the dosage and treatment frequency of the conjugated cells before evaluation in humans. In general, given the versatility of polydopamine in presenting structurally diverse molecules, we anticipate widespread use of this method as a safe and universal platform for vaccine development against new infectious diseases.

Author statement

All data needed to evaluate the conclusions in the paper are present in the paper and/or the Supplementary Materials. Additional data related to this paper are available from the authors upon reasonable request.

Declaration of Competing Interest

The authors declare that they have no known competing financial interests or personal relationships that could have appeared to influence the work reported in this paper.

Acknowledgements

This work was financially supported by the National Natural Science Foundation of China (21875135), the Recruitment Program of Global Youth Experts of China (D1410022), the Shanghai Municipal Education Commission-Gaofeng Clinical Medicine Grant Support (20181704, 20191820), and the Innovative Research Team of High-level Local Universities in Shanghai (SSMU-ZLCX20180701).

Appendix A. Supporting information

Supplementary data associated with this article can be found in the online version at doi:10.1016/j.nantod.2021.101280.

References

[1] E. Hammarlund, M.W. Lewis, S.G. Hansen, L.I. Strelow, J.A. Nelson, G.J. Sexton, J.M. Hanifin, M.K. Slifka, Duration of antiviral immunity after smallpox vaccination, Nat. Med. 9 (2003) 1131–1137.
[2] D.R. Burton, R. Ahmed, D.H. Barouch, S.T. Butera, S. Crotty, A. Godzik, D.E. Kaufmann, M.J. McElrath, M.C. Nussenzweig, B. Pulendran, C.N. Scanlan, W.R. Schief, G. Silvestri, H. Streeck, B.D. Walker, L.M. Walker, A.B. Ward, I.A. Wilson, R. Wyatt, A blueprint for HIV vaccine discovery, Cell Host Microbe 12 (2012) 396–407.
[3] C.Y. Yong, H.K. Ong, S.K. Yeap, K.L. Ho, W.S. Tan, Recent advances in the vaccine development against Middle East respiratory syndrome-coronavirus, Front. Microbiol. 10 (2019) 1781.
[4] WHO, https://www.who.int/publications/m/item/weekly-epidemiological-update-on-covid-19–13-april-2021, 2020.
[5] Z. Zhang, Z. Tang, N. Farokhzad, T. Chen, W. Tao, Sensitive, rapid, low-cost, and multiplexed COVID-19 monitoring by the wireless telemedicine platform, Matter 3 (2020) 1818–1820.
[6] M. Day, Covid-19: four fifths of cases are asymptomatic, China figures indicate, BMJ 369 (2020) 1375.
[7] M.D. Shin, S. Shukla, Y.H. Chung, V. Beiss, S.K. Chan, O.A. Ortega-Rivera, D.M. Wirth, A. Chen, M. Sack, J.K. Pokorski, N.F. Steinmetz, COVID-19 vaccine development and a potential nanomaterial path forward, Nat. Nanotechnol. 15 (2020) 646–655.
[8] X. Zhou, X. Jiang, M. Qu, G.E. Aninwene, V. Jucaud, J.J. Moon, Z. Gu, W. Sun, A. Khademhosseini, Engineering antiviral vaccines, ACS Nano 14 (2020) 12370–12389.
[9] J.J. Bull, Evolutionary reversion of live viral vaccines: can genetic engineering subdue it? Virus Evol. 1 (2015) vev005.
[10] R.L. Coffman, A. Sher, R.A. Seder, Vaccine adjuvants: putting innate immunity to work, Immunity 33 (2010) 492–503.
[11] D.H. Barouch, M.G. Pau, J.H. Custers, W. Koudstaal, S. Kostense, M.J. Havenga, D.M. Truitt, S.M. Sumida, M.G. Kishko, J.C. Arthur, B. Korioth-Schmitz, M.H. Newberg, D.A. Gorgone, M.A. Lifton, D.L. Panicali, G.J. Nabel, N.L. Letvin, J. Goudsmit, Immunogenicity of recombinant adenovirus serotype 35 vaccine in the presence of pre-existing anti-Ad5 immunity, J. Immunol. 172 (2004) 6290–6297.
[12] A. Amoscato, D.A. Prenovitz, M.T. Lotze, Rapid extracellular degradation of synthetic class I peptides by human dendritic cells, J. Immunol. 161 (1998) 4023–4032.
[13] A. Pietroiusti, L. Campagnolo, B. Fadeel, Interactions of engineered nanoparticles with organs protected by internal biological barriers, Small 9 (2013) 1557–1572.
[14] D.M. Smith, J.K. Simon, J.R. Baker Jr., Applications of nanotechnology for immunology, Nat. Rev. Immunol. 13 (2013) 592–605.
[15] M.S. Goldberg, Improving cancer immunotherapy through nanotechnology, Nat. Rev. Cancer 19 (2019) 587–602.
[16] G. Chauhan, M.J. Madou, S. Kalra, V. Chopra, D. Ghosh, S.O. Martinez-Chapa, Nanotechnology for COVID-19: therapeutics and Vaccine Research, ACS Nano 14 (2020) 7760–7782.
[17] Y.H. Chung, V. Beiss, S.N. Fiering, N.F. Steinmetz, COVID-19 vaccine frontrunners and their nanotechnology design, ACS Nano 14 (2020) 12522–12537.
[18] P. Lung, J. Yang, Q. Li, Nanoparticle formulated vaccines: opportunities and challenges, Nanoscale 12 (2020) 5746–5763.
[19] E.J. Bohnsack Jf Fau - Brown, E.J. Brown, The role of the spleen in resistance to infection, Annu. Rev. Med. 37 (1986) 49–59.
[20] F.D. Batista, N.E. Harwood, The who, how and where of antigen presentation to B cells, Nat. Rev. Immunol. 9 (2009) 15–27.
[21] T.R. Klei, S.M. Meinderts, T.K. van den Berg, R. van Bruggen, From the cradle to the grave: the role of macrophages in erythropoiesis and erythrophagocytosis, Front. Immunol. 8 (2017) 73.
[22] H. Minasyan, Mechanisms and pathways for the clearance of bacteria from blood circulation in health and disease, Pathophysiology 23 (2016) 61–66.
[23] H. Minasyan, Phagocytosis and oxycytosis: two arms of human innate immunity, Immunol. Res. 66 (2018) 271–280.
[24] D. de Back, E. Kostova, M. van Kraaij, T. van den Berg, R. Van Bruggen, Of macrophages and red blood cells; a complex love story, Front. Physiol. 5 (2014) 9.
[25] J.S. Brenner, D.C. Pan, J.W. Myerson, O.A. Marcos-Contreras, C.H. Villa, P. Patel, H. Hekierski, S. Chatterjee, J.-Q. Tao, H. Parhiz, K. Bhamidipati, T.G. Uhler, E.D. Hood, R.Y. Kiseleva, V.S. Shuvaev, T. Shuvaeva, M. Khoshnejad, I. Johnston, J.V. Gregory, J. Lahann, T. Wang, E. Cantu, W.M. Armstead, S. Mitragotri, V. Muzykantov, Red blood cell-hitchhiking boosts delivery of nanocarriers to chosen organs by orders of magnitude, Nat. Commun. 9 (2018) 2684.
[26] K. Danielyan, K. Ganguly, B.-S. Ding, D. Atochin, S. Zaitsev, J.-C. Murciano, P.L. Huang, S.E. Kasner, D.B. Cines, V.R. Muzykantov, Cerebrovascular thromboprophylaxis in mice by erythrocyte-coupled tissue-type plasminogen activator, Circulation 118 (2008) 1442–1449.
[27] N. Pishesha, A.M. Bilate, M.C. Wibowo, N.-J. Huang, Z. Li, R. Deshycka, D. Bousbaine, H. Li, H.C. Patterson, S.K. Dougan, T. Maruyama, H.F. Lodish, H.L. Ploegh, Engineered erythrocytes covalently linked to antigenic peptides can protect against autoimmune disease, Proc. Natl. Acad. Sci. USA 114 (2017) 3157–3162.
[28] A. Ukidve, Z. Zhao, A. Fehnel, V. Krishnan, D.C. Pan, Y. Gao, A. Mandal, V. Muzykantov, S. Mitragotri, Erythrocyte-driven immunization via biomimicry of their natural antigen-presenting function, Proc. Natl. Acad. Sci. USA 117 (2020) 17727–17736.
[29] N.W. Daniel Wrapp, Kizzmekia S. Corbett, Jory A. Goldsmith, Ching-Lin Hsieh, Olubukola Abiona, Barney S. Graham, Jason S. McLellan, Cryo-EM structure of the 2019-nCoV spike in the prefusion conformation, Science 367 (2020) 1260–1263.
[30] Y.Z. Renhong Yan, Yaning Li, Lu Xia, Yingying Guo, Qiang Zhou, Structural basis for the recognition of SARS-CoV-2 by full-length human ACE2, Science 367 (2020) 1444–1448.
[31] D. Benvenuto, M. Giovanetti, A. Ciccozzi, S. Spoto, S. Angeletti, M. Ciccozzi, The 2019-new coronavirus epidemic: evidence for virus evolution, J. Med. Virol. 92 (2020) 455–459.

[32] E. Prompetchara, C. Ketloy, T. Palaga, Immune responses in COVID-19 and potential vaccines: lessons learned from SARS and MERS epidemic, Asian Pac. J. Allergy Immunol. 38 (2020) 1–9.
[33] Z.-x Zhou, L. Sun, Immune effects of R848: evidences that suggest an essential role of TLR7/8-induced, Myd88- and NF-κB-dependent signaling in the antiviral immunity of Japanese flounder (Paralichthys olivaceus), Dev. Comp. Immunol. 49 (2015) 113–120.
[34] S. McCartney, W. Vermi, S. Gilfillan, M. Cella, T.L. Murphy, R.D. Schreiber, K.M. Murphy, M. Colonna, Distinct and complementary functions of MDA5 and TLR3 in poly(I:C)-mediated activation of mouse NK cells, J. Exp. Med. 206 (2009) 2967–2976.
[35] M.A. Moody, S. Santra, N.A. Vandergrift, L.L. Sutherland, T.C. Gurley, M.S. Drinker, A.A. Allen, S.-M. Xia, R.R. Meyerhoff, R. Parks, K.E. Lloyd, D. Easterhoff, S.M. Alam, H.-X. Liao, B.M. Ward, G. Ferrari, D.C. Montefiori, G.D. Tomaras, R.A. Seder, N.L. Letvin, B.F. Haynes, Toll-like receptor 7/8 (TLR7/8) and TLR9 agonists cooperate to enhance HIV-1 envelope antibody responses in rhesus macaques, J. Virol. 88 (2014) 3329–3339.
[36] H.F. Florindo, R. Kleiner, D. Vaskovich-Koubi, R.C. Acúrcio, B. Carreira, E. Yeini, G. Tiram, Y. Liubomirski, R. Satchi-Fainaro, Immune-mediated approaches against COVID-19, Nat. Nanotechnol. 15 (2020) 630–645.
[37] N. Wang, Y. Yang, X. Wang, X. Tian, W. Qin, X. Wang, J. Liang, H. Zhang, X. Leng, Polydopamine as the antigen delivery nanocarrier for enhanced immune response in tumor immunotherapy, ACS Biomater. Sci. Eng. 5 (2019) 2330–2342.
[38] Q. Ye, F. Zhou, W. Liu, Bioinspired catecholic chemistry for surface modification, Chem. Soc. Rev. 40 (2011) 4244–4258.
[39] D. Pan, O. Vargas-Morales, B. Zern, A.C. Anselmo, V. Gupta, M. Zakrewsky, S. Mitragotri, V. Muzykantov, The effect of polymeric nanoparticles on biocompatibility of carrier red blood cells, PLOS One 11 (2016) 0152074.
[40] J. Banchereau, R.M. Steinman, Dendritic cells and the control of immunity, Nature 392 (1998) 245–252.
[41] P. Guermonprez, J. Valladeau, L. Zitvogel, C. Théry, S. Amigorena, Antigen presentation and T cell stimulation by dendritic cells, Annu. Rev. Immunol. 20 (2002) 621–667.
[42] A. Savina, S. Amigorena, Phagocytosis and antigen presentation in dendritic cells, Immunol. Rev. 219 (2007) 143–156.
[43] Q. Liu, J. Jia, T. Yang, Q. Fan, L. Wang, G. Ma, Pathogen-mimicking polymeric nanoparticles based on dopamine polymerization as vaccines adjuvants induce robust humoral and cellular immune responses, Small 12 (2016) 1744–1757.
[44] F. Borriello, M.P. Sethna, S.D. Boyd, A.N. Schweitzer, E.A. Tivol, D. Jacoby, T.B. Strom, E.M. Simpson, G.J. Freeman, A.H. Sharpe, B7-1 and B7-2 have overlapping, critical roles in immunoglobulin class switching and germinal center formation, Immunity 6 (1997) 303–313.
[45] G.H. Matundan H, Herpes simplex virus 1 ICP22 suppresses CD80 expression by murine dendritic cells, J. Virol. 93 (2019) 1803–1818.
[46] D. Wen, J. Wang, G. Van Den Driessche, Q. Chen, Y. Zhang, G. Chen, H. Li, J. Soto, M. Liu, M. Ohashi, Z. Wang, P. Abdou, Q. Hu, G. Dotti, S. Li, D. Fourches, Z. Gu, Adipocytes as anticancer drug delivery depot, Matter 1 (2019) 1203–1214.
[47] R.D. Weeratna, M.J. McCluskie, Y. Xu, H.L. Davis, CpG DNA induces stronger immune responses with less toxicity than other adjuvants, Vaccine 18 (2000) 1755–1762.
[48] L.L. Thomsen, P. Topley, M.G. Daly, S.J. Brett, J.P. Tite, Imiquimod and resiquimod in a mouse model: adjuvants for DNA vaccination by particle-mediated immunotherapeutic delivery, Vaccine 22 (2004) 1799–1809.
[49] S.N. Shishido, S. Varahan, K. Yuan, X. Li, S.D. Fleming, Humoral innate immune response and disease, Clin. Immunol. 144 (2012) 142–158.
[50] M. Zimmermann, N. Rose, J.M. Lindner, H. Kim, A.R. Gonçalves, I. Callegari, M. Syedbasha, L. Kaufmann, A. Egli, R.L.P. Lindberg, L. Kappos, E. Traggiai, N.S.R. Sanderson, T. Derfuss, Antigen extraction and B cell activation enable identification of rare membrane antigen specific human B cells, Front. Immunol. 10 (2019) 829.
[51] M. Stebegg, S.D. Kumar, A. Silva-Cayetano, V.R. Fonseca, M.A. Linterman, L. Graca, Regulation of the germinal center response, Front. Immunol. 9 (2018) 2469.
[52] W.-j Guan, Z.-y Ni, Y. Hu, W.-h Liang, C.-q Ou, J.-x He, L. Liu, H. Shan, C.-l Lei, D.S.C. Hui, B. Du, L.-j Li, G. Zeng, K.-Y. Yuen, R.-c Chen, C.-l Tang, T. Wang, P.-y Chen, J. Xiang, S.-y Li, J.-l Wang, Z.-j Liang, Y.-x Peng, L. Wei, Y. Liu, Y.-h Hu, P. Peng, J.-m Wang, J.-y Liu, Z. Chen, G. Li, Z.-j Zheng, S.-q Qiu, J. Luo, C.-j Ye, S.-y Zhu, N.-s Zhong, Clinical characteristics of coronavirus disease 2019 in China, N. Engl. J. Med. 382 (2020) 1708–1720.
[53] M.Z. Tay, C.M. Poh, L. Rénia, P.A. MacAry, L.F.P. Ng, The trinity of COVID-19: immunity, inflammation and intervention, Nat. Rev. Immunol. 20 (2020) 363–374.
[54] D.A. Chesler, C.S. Reiss, The role of IFN-gamma in immune responses to viral infections of the central nervous system, Cytokine Growth Factor Rev. 13 (2002) 441–454.
[55] G. Mancuso, A. Midiri, C. Biondo, C. Beninati, S. Zummo, R. Galbo, F. Tomasello, M. Gambuzza, G. Macrì, A. Ruggeri, T. Leanderson, G. Teti, Type I IFN signaling is crucial for host resistance against different species of pathogenic bacteria, J. Immunol. 178 (2007) 3126–3133.
[56] C.E. Samuel, Antiviral actions of interferons, Clin. Microbiol. Rev. 14 (2001) 778–809.
[57] M. Haji Abdolvahab, S. Moradi-kalbolandi, M. Zarei, D. Bose, K. Majidzadeh-A, L. Farahmand, Potential role of interferons in treating COVID-19 patients, Int. Immunopharmacol. 90 (2021) 107171.
[58] C.-M.J. Hu, R.H. Fang, L. Zhang, Erythrocyte-inspired delivery systems, Adv. Healthc. Mater. 1 (2012) 537–547.
[59] K. Yang, J.S. Lee, J. Kim, Y.B. Lee, H. Shin, S.H. Um, J.B. Kim, K.I. Park, H. Lee, S.-W. Cho, Polydopamine-mediated surface modification of scaffold materials for human neural stem cell engineering, Biomaterials 33 (2012) 6952–6964.